Dynamic Dose Determination in a Gamma Irradiator using PHITS Monte Carlo Code: Transit Dose

Intan Nafisah [1, 2, a)], Bimo Saputro[2, 3], Okky Agassy Firmansyah[2], Zhongming Zhang [4] , Dian Adi Prastowo[2], Fendinugroho[2], Fifi Nurfiana[2], Waringin Margi Yusmaman[2]

Author Affiliations

[1]*University of Birmingham*
(Edgbaston, Birmingham, B15 2TT United Kingdom)
[2]*National Research and Innovation Agency (BRIN Indonesia)*
(*BJ Habibie Science Complex, Serpong, Muncul, Tangerang Selatan, Kota Tangerang Selatan, Banten 15310*).
[3]*University of Indonesia*
(Faculty of Mathematics and Natural Sciences, University of Indonesia, UI Depok Campus, West Java 16424)
[4]*Lancaster University*
(School of Engineering, Engineering Building, Lancaster University, LA1 4YW United Kingdom)

Author Emails
[a)] Corresponding author: inta014@brin.go.id

Abstract

Gamma irradiation facilities have been widely utilised for various sectors, including healthcare, agriculture, and material science. Therefore, it is crucial to understand the dose rate distribution within the chamber to ensure the samples receive the prescribed dose. PHITS Monte Carlo code was employed to simulate a self-shielded gamma irradiator category I. The facility features 36 pencil sources of Co-60 that are arranged around the sample chamber. A three-dimensional model of the gamma irradiator was developed using the PHITS Monte Carlo Code to simulate photon transport and dose deposition, while dynamic dose components during chamber movement were estimated using Simpson's numerical integration. Validation using alanine dosimetry yielded a good agreement (2.4% relative difference), confirming the model's accuracy and reliability. The dose map revealed the heterogeneity for both radial and axial distribution along the central axis. The highest differences in dose rate distribution were~ 40% radially and ~45% axially. Therefore, to achieve a more uniform dose distribution (ratio ~1.1), it is suggested that the samples are placed at a height between 8 and 21 cm. The Simpson's integration method was implemented to bridge the gap between discrete simulations and dynamic physical processes for transit dose determination. The simulation calculated a transit dose of approximately 1.9 Gy with an uncertainty of 0.16% at the chamber's centre-bottom position for one irradiation cycle.

Keywords: Dosimetry, gamma irradiator, Monte Carlo, transit dose.

1. Introduction

The heterogeneous dose distribution presents a significant challenge in operating a self-contained dry-gamma source irradiator. The absorbed dose inside the sample chamber of the irradiator may vary considerably, which is an essential concern to achieve the prescribed dose (Farah et al., 2025). In the previous study, the variation can reach up to 20% and 26% for radial and axial directions (Moradi et al., 2017). Consequently, it is essential to find the dose distribution of the chamber to guarantee that the sample receives the required dose (Oliveira, et al., 2000; Aknouch et al., 2020). Accurately knowing the dose distribution helps in selecting the optimum irradiation location, which optimises the irradiation time. Thus, the delivered dose to the material can be estimated and controlled (Hefue, 2000; Jecong et al., 2022). By the experiment, dose distribution can be determined by placing dosimeters at different positions in the irradiation chamber (Saputro et al., 2024). This method is limited to the specific locations where the dosimeters are positioned. Adding the dosimeters improves the accuracy of the experimental dose rate. However, locating the dosimeters with a close gap to provide a complete mapping is impractical in an irradiation chamber (Jecong et al., 2022). Monte Carlo is a powerful and effective method to simulate photon interactions with matter and create a precise geometry and characteristics of the experimental irradiation conditions (Mortuza et al., 2018).

Simulating certain dynamic industrial processes presents complex technical challenges. For instance, demonstrating axial translation and rotation during the irradiation process is difficult because most three-dimensional Monte Carlo simulations rely on a static geometric approach (Gual et al., 2019). This static approach might be one challenge in determining transit dose. Transit dose is the dose received during the movement of the sample chamber to the irradiation position and returning to its storage/secure position (El-ouardi et al., 2023; Majer et al., 2019). This dose is usually neglected when dealing with industrial irradiators, which require a high absorbed dose. However, in the case of a small geometry and at low dose operation, the transit dose has a significant influence, especially for high dose rates (HTR)(Follett, 2004; Guzmán Calcina et al., 2005; Wojcicka et al., 1999). In the case of HDR, the sample will be accumulated with the dynamic dose received during its movement into the irradiation area, the absorbed dose will be higher than the prescribed dose, resulting in a significant impact for low-dose processes (A. C. Gonçalves et al., 2022). The transit dose depends on the activity of the source, treatment fractions, and target speed (Mannai et al., 2007). Therefore, the estimation of the transit dose is essential for the quality control process(Feldmann et al., 2019; Fitriana et al., 2024).

Despite the growing interest in Monte Carlo simulation for dose mapping in a gamma irradiator, the comprehensive utilisation of PHITS remains limited for dynamic movement either for sample or sources. This regard to determine transit dose. Monte Carlo like PHITS represent a static geometrical configuration, where the particles are transported within a fixed spatial environment for each batch simulation (Bento et al., 2012; Watabe et al., 2024). Due to the lack 4D model in continuous spatial

transitions of sources or targets during simulation, it is necessary to bridge the gap between static and dynamic scenario using external processing (Sato et al., 2018, 2024). Various methodologies for quantifying transit doses rely on a combination of experimental and computational frameworks. Experimental approaches typically utilise cumulative and linear regression techniques (Farah et al., 2025). While the cumulative method measures the dose accumulated during a series of source position exposures, linear regression establishes the relationship between absorbed dose and irradiation time to derive the transit dose from the y-intercept. Conversely, standard computational methods using Monte Carlo codes employ discrete step-by-step simulation strategies, translating the source or target through a series of finite spatial increments (Mannai et al., 2007). In contrast, the GATE code provides an alternative by allowing for continuous geometry movement during the simulation (El-ouardi et al., 2023).

This study fills the gap methodologies for calculating the transit dose through dynamic Monte Carlo code. By using a polynomial approach to interpolate the radiation field, we expect to achieve higher accuracy and a more refined representation of the dose curve. The objectives of this study are: (1) to validate the PHITS calculation with the experimental data using alanine dosimetry; (2) to map the radial and axial dose distribution within the centre plane of the chamber; (3) to calculate and evaluate the transit dose at the centred-bottom level using Simpson integration method. The insights gained from this study provide a mathematical approach for evaluating achieved dose in moving products. Ultimately, this approach enables more accurate determination of maximum and minimum doses, allowing for the optimisation of sample placement and enhanced the efficiency in irradiation timing.

2. Materials and methods

2.1 Irradiation Facility

The Observo Ignis gamma irradiation facility was manufactured by the Institute of Isotopes Co. Ltd, Budapest. It is a dry-self-shielded (category I) gamma irradiator facility. Figure 1 below shows the self-contained dry storage irradiator. The installation of this facility was on December 5th, 2017. A thick shielding covers the irradiation area, which is also a place for the gamma sources. The source configuration in the simulation is made according to real conditions, where each pencil source describes the specific activity of cobalt-60. Geometry entails defining the simulation space's geometry, including the dimensions, forms, and composition of all pertinent parts. The inner chamber was modelled containing dry air and a structured arrangement of alanine dosimeters to simulate dose distribution within the geometry. The internal volume of the sample chamber was modelled as dry air to maintain strict consistency with the atmospheric conditions of the experimental facility, ensuring that attenuation and scattering effects were accurately represented.

Figure 1 Self-contained Irradiator Category one (Model: Ob-Servo Ignis Research Gamma Irradiator, Manufacturer: Izotop Institute of Isotopes).

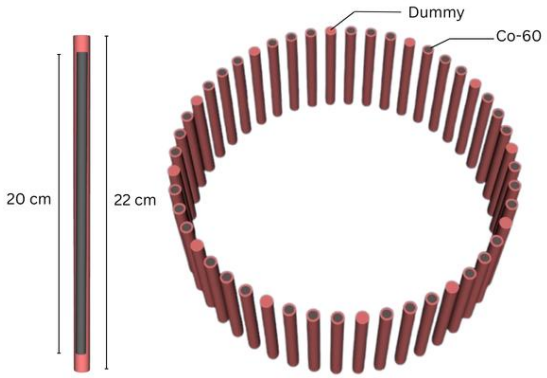

Figure 2 Schematic representation of the chamber's internal geometry and source radial alignment (upper view).

The gamma sources have a circular arrangement with 48 pencil positions. Currently, 36 positions contain Co-60, the remaining 12 pencils are dummies or have no isotopes. The overall dimensions are 22 cm in length and 1.1 cm in diameter, with an active dimension inside of 20 cm in length and 0.72 cm in diameter. The sample chamber is a thin-walled, non-corrosive metal of stainless steel, which is positioned between the moving central plugs. It is raised to the loading and unloading position via a pneumatic drive motor. The chamber goes down in the irradiation position align with the vertical axis, which brings the sample to the irradiation area. The dimensions of the chamber are 15 cm in diameter and 28 cm in height. Samples up to 5 litres can be accommodated in the chamber. In this study, the Monte Carlo model focuses solely on the sample chamber rather than the entire irradiator. Figure 2 illustrates the position of the sources and the sample chamber. The pitch circle diameter of the source is 29 cm, which is the distance from centre to centre of the two furthest pencils. The source consists of 36 cobalt-60 pencils encapsulated in stainless steel (SS 304). The total activity of the source was 12.05 kCi (445.85 TBq) on the initial date of October 6th, 2017. In addition, the Observo Irradiator was calibrated in terms of absorbed dose to water by in-plant method. The calibration performed by RisØ High Dose Reference Laboratory of DTU Health Technology, which is traceable to the national standard at National Physical Laboratory (NPL), United Kingdom.

2.2 Dosimetry System

This study utilised Harwell alanine pellet dosimeters measuring 4.8 mm in diameter and 2.8 mm in thickness. Calibrated in terms of absorbed dose to water at the National Physical Laboratory (NPL), the pellets were read using an ADVIN (Belarus) electron spin resonance (ESR) spectrometer. The measurements carried an expanded uncertainty of 4.5% (k=2 at a 95% confidence level), factoring in contributions from the ESR spectrometer, alanine dosimeter, weight (balance), and thermometer.

According to the NPL calibration certificate, the primary contributors to this uncertainty were the absorbed dose alanine uncertainty and the ESR dose measurement accuracy(Nanez & Uribe, 2023).

2.3 Experimental Validation

The PHITS Monte Carlo model was validated by comparing in situ experimental measurements from the alanine dosimeter with the simulation results. The dose rate from the PHITS calculation was the average result of four alanine pellets positioned vertically in the centre of the sample's chamber. The dosimeter was positioned at the centre of the sample chamber in a similar location to that during the calibration. Relative Dose Difference (RDD) was implemented to assess the difference between the experimental measurement using dosimeters and the PHITS calculation. The lower the RDD result, the closer the simulation calculation is to the experimental data. The RDD formula can be found as follows:

$$Relative\ Dose\ Difference\ (RDD) = \frac{|simulated\ dose - measured\ dose|}{measured\ dose} \times 100\% \quad (1)$$

2.4 PHITS simulations

PHITS version 3.35 was employed in this study to simulate and calculate the absorbed dose. A 3D model was developed using PHITS version 3.35, as depicted in Figure 3, using the PHITS 3D compiler. The geometrical details and all material compositions in accordance with the experimental situation were modelled in the simulation for a precise result. This simulation study of this facility has never been conducted before, so that the benchmark studies will be performed with a similar type of irradiator. Additionally, the focus of this study will be limited to the radiation in the sample chamber and the pencil sources. Compendium material 2021 was used to define the standard density for materials in the simulation, such as stainless steel 304, water, air, cobalt, polystyrene foam, and polymethyl methacrylate.

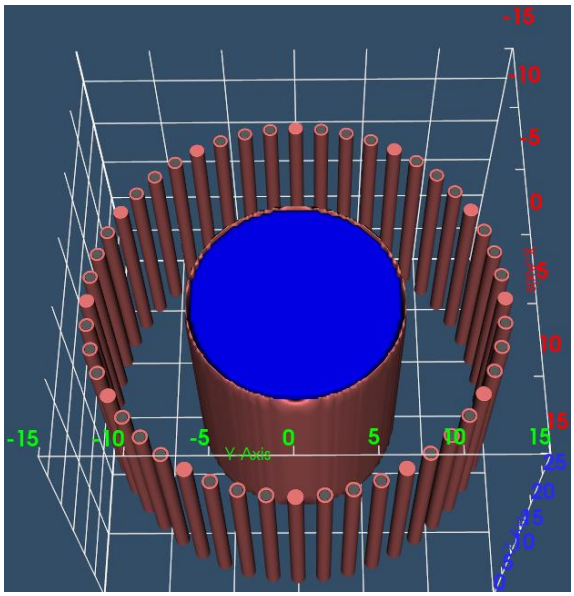

Figure 3 3D model of gamma irradiation facility using PHITS 3D compiler.

In addition, Co-60 pencils with exact positions and activity have been placed according to the certificate information. In the source section, a pencil of Co-60 source was modelled in a cylindrical rod, and the isotope part was wrapped by SS304-Steel. There was a dummy source located every 30°, thus a total of 12 solid stainless-steel pencils were installed. In this study, the direction of the source particles was isotropic. The Co-60 source was defined as a radioisotope using *e-type = 28* parameter. This explicitly accounts for the two distinct gamma-ray energy peaks at 1.17 MeV and 1.33 MeV, as well as the associated beta-particle emissions. In the scoring section, users can arrange any desired calculations, for instance, T-track and T-deposit. T-track was used to calculate the flux in a particular region, while T-deposit was utilised to measure energy deposited in a specific area, for example, at options XYZ, RZ, and Reg. In addition, the unit of the T-deposit is Gy/hour. In this present study, 10^9 to $2x10^9$ particles were generated to achieve a low statistical uncertainty of less than 5%(Kim et al., 2015). A parameter of *Negs = 1* was utilised to enable the EGS5 mode, allowing for the transport of photons, electrons, and positrons. The energy cut-off values were set at 1 keV for photons and 0.1 MeV for both electrons and positrons.

2.5 Transit Dose Calculation

To measure the transit dose, the alanine dosimeters were exposed to the irradiator sources during repeated up-and-down cycles without any additional irradiation time programmed. The measurements had been repeated ten times. On the other hand, PHITS operates within a steady-state framework to solve the Boltzmann radiation transport equations. Consequently, modelling dynamic scenarios, such as the continuous movement of cells or sources, is a challenge within this time-independent framework. Considering that the transit dose is an accumulated dose while the sample is passing through different positions, numerical integration must be used to quantify this dose. This technique breaks down the area under the curve into small shapes, such as trapezoids, and sums up all the areas to get the total quantity (Mannai et al., 2007). The chamber's speed is constant (11.4 cm/s). The Simpson method is utilised as it establishes a parabolic relation between three consecutive points, leading to a more accurate approximation of the area under the curve. The following formula defines the Simpson rule(Chapra & Canale, 2010).

$$I = \int_a^b f(x)dx$$

$$I \approx \left(h/3\right)[f(x_0) + 4\sum odd\ index\ terms + 2\sum even\ index\ terms + f(x_{2n})] \quad (2)$$

The uncertainty for the dynamic dose evaluation considers the statistical uncertainty originating from PHITS Monte Carlo calculations. The total variance of the integrated transit dose (I) was evaluated by propagating these uncertainties through the Simpson's 1/3 integration scheme. Assuming that the

discrete simulation tallies are completely uncorrelated, Eq. 3 defines the error propagation for the accumulated error associated from the integration:

$$\sigma_I{}^2 = \frac{1}{9}h^2\left[f_{x0}{}^2 + 16\sum(f_{odd})^2 + 4\sum(f_{even})^2 + f_{x_{2n}}{}^2\right] \quad (3)$$

where h represents the step size, and f denotes the statistical uncertainty of the PHITS simulation results at each discrete spatial interval.

3. Result and discussion

3.1 Monte Carlo Model Validation

The dose rate obtained by PHITS simulation was 2.9 kGy/h, with a statistical error of 1.6%. The dose rate then multiplied by nine irradiation time. The PHITS simulation showed a promising agreement with the nine measurements using traceable alanine dosimeters. Figure 4 compares the PHITS simulation data to the experimental measurement. The dose rate measured by the alanine dosimeters in the irradiator was 2.9 kGy/h. The simulation and experimental data results were normalised using the dose gained from the calibration curve from the same allocation time. RDD was derived from the difference between values recorded from PHITS and alanine dosimeter reader.

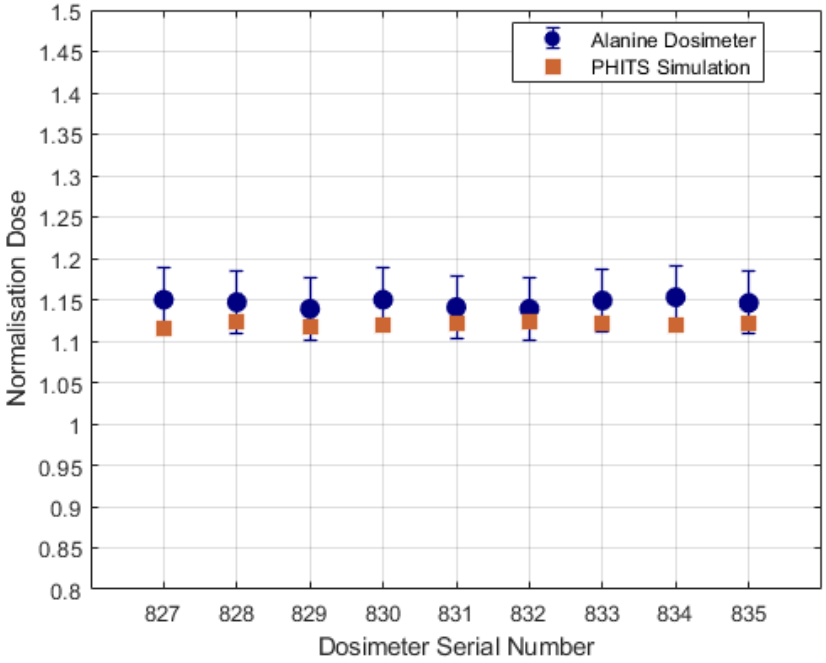

Figure 4 Comparison between PHITS Simulation and Alanine Dosimeters Measurements. The relative differences were lower than 3%.

The previous study by Firmansyah et al (Firmansyah, Kurniawan, Walo, et al., 2025), which used PHITS and alanine dosimeters, showed a discrepancy of 7%, it was higher than that observed in the present study. This improvement could be achieved by constructing the geometry similar to the real facility, detailed optimisation of decay time, and defining the material structure as similar to the real materials. The linearity curve of dose (Y axis) and irradiation time (X axis) resulted in the dose rate of

the experimental measurement. It produced a 2.4% relative dose difference between the simulation and experiment dose rate. Table 1 presents the dose rates of both measurements.

Table 1 Dose Rate Difference between PHITS and Experimental Measurement

Category	Dose rate (kGy/h)	Uncertainty (%)
PHITS Simulation	2.9	1.6
Alanine Dosimeter	2.9	3.3
RDD	2.4%	

To maintain consistency with the estimated experimental uncertainty (which is reported to two significant figures), both dose rates have been rounded accordingly. Consequently, the rounded experimental and simulated values appear identical. The RDD between the unrounded raw data sets was 2.4%, demonstrating strong agreement between the model and the physical measurement.

3.2 Radial Dose Distribution across Chamber's Diameter

The determination of radial dose rate was scored by T-deposit using the x-axis mesh type. The diameter of the 15 cm sample chamber was divided by 75 meshes. It created a 2 mm width of each mesh located in the centre of chamber (Y=0).

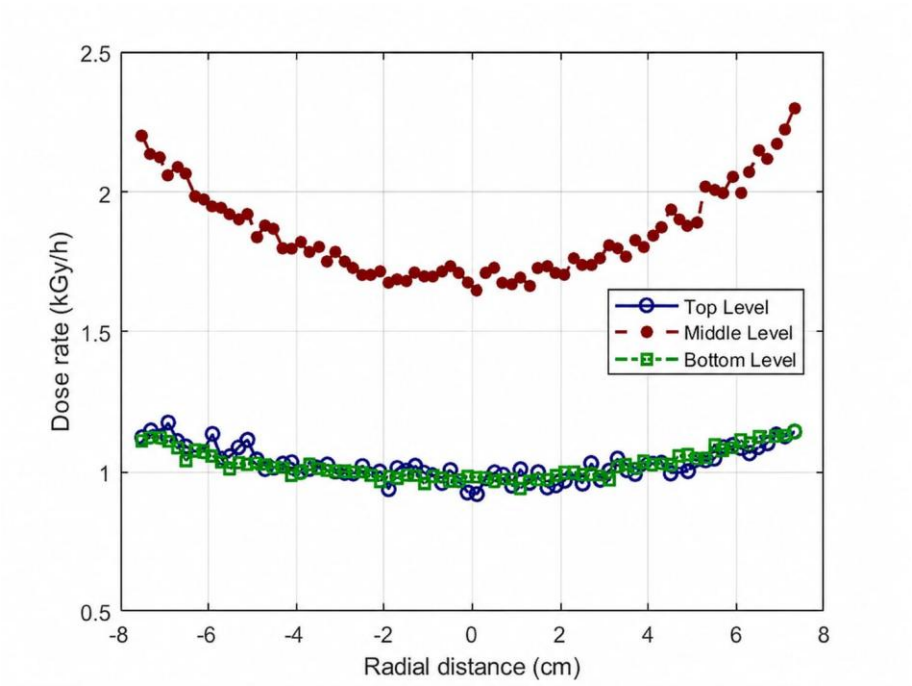

Figure 5 Radial dose rate on the central axis of the sample chamber in three height levels. Dose rates at the edge of the chamber were 18%-40% higher than at the central point.

Figure 5 shows the dose profile on the radial axis across the diameter of the chamber at the top, middle, and bottom heights of the chamber. The mesh spanning the diameter of the chamber calculated higher doses near the chamber wall and lower in the centre. From the figure, the dose rate in the centre axis of the chamber varied with height and distance from the chamber's wall. The dose rate at the centre of the

chamber was lower compared to the edges which was close to the chamber's wall. The trend in dose rate along the radial-centrical plane was similar to those reported in previous research (Farah et al., 2025; Moradi et al., 2017). The difference between the edge (highest) and centre (lowest) dose rate was roughly 27% in the top level and 18% in the bottom level.

Conversely, at mid-height, there was a clear attenuation of dose rate towards the centre of the chamber. The dose rates were approximately 1.6 kGy/h in the centre and 2.3 kGy/h at the chamber's edge (statistical error = 1.9%), which was ~40% higher. In other words, the Dose Uniformity Ratio (DUR) was approximately 1.4 throughout the line. This ratio indicated the dose near the chamber wall was 140% of the dose at the centre of the chamber. The DUR, representing the ratio between the maximum and minimum doses within the irradiation chamber (Aknouch et al., 2021). A significant radial gradient was a result of gamma attenuation: the sample in the centre was further from the Co-60 pencil source, resulting in a lower dose. Additionally, Figure 6 shows absorbed dose distribution within the chamber along the X and Y axes. The figure depicts that higher absorbed dose was located near the source. To obtain a DUR of 1.1, the sample should be irradiated at a radius of 5 cm from the centre.

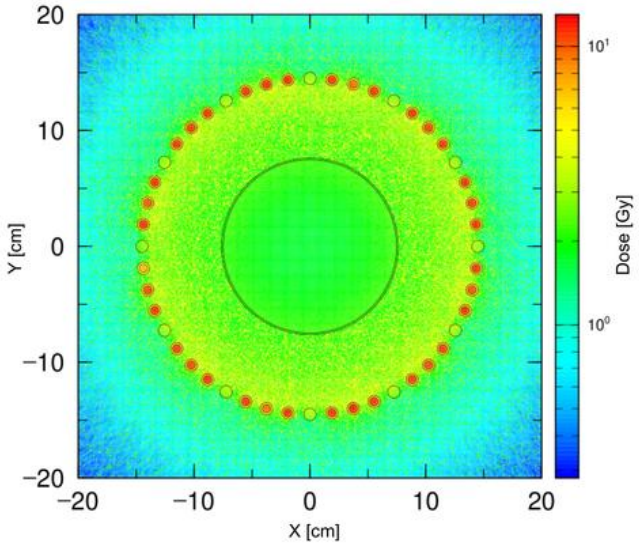

Figure 6 Dose distribution along the XY-plane exhibits a lower trend in the inner area of the chamber.

3.3 Axial Dose Distribution across Chamber's Height

The dose rate distribution along the axial direction was evaluated via the T-deposit tally, employing an RZ mesh with a radius adjusted to 0.5 cm from the centre of the sample chamber. This volume was divided into 140 meshes for a sample chamber height of 28 cm. Therefore, each mesh had a width of 2 mm. Figure 7 describes the variation of dose rate along the axial position. The highest dose rate was located in the central area. This higher dose was due to the location of the pencil sources, which were placed in the middle of the irradiation chamber. The central part has a larger solid angle, which implies receiving higher radiation exposure from various angles, as shown in Figure 7. Additionally, this configuration affects the upper and lower levels of the chamber, which acquires a significantly

lower dose rate than the middle level. Both dose rates were approximately 1.0 kGy/h, with associated statistical uncertainties of up to 1.9%. Both only obtain approximately ~55% of the dose rate at the middle level (1.7 kGy/hr). The upper and lower levels were not exposed by the source as intensely as the middle part. A lower radiation dose rate is due to a further distance to the source, indicating the inverse square law of radiation. The decreasing trend at the upper and lower levels was similar to that reported in the literature (Dridi et al., 2020; Farah et al., 2025; Mannai et al., 2007; Moradi et al., 2017).

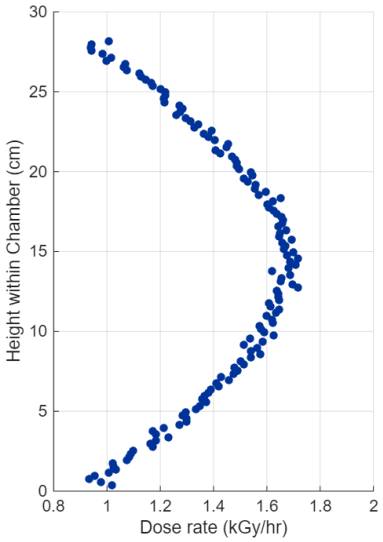

Figure 7 Axial Dose Rate Distribution as a function of Sample Chamber's Height, Showing Peak Intensity at Approximately 15 cm.

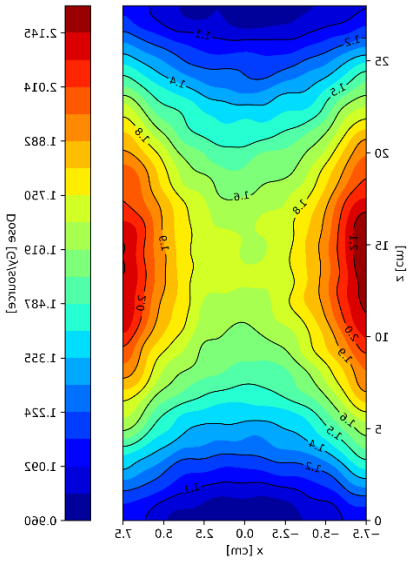

Figure 8 The isodose distribution within the chamber's height. The maximum dose was concentrated at the centre (z=15), reflected the optimal geometric exposure relative to the full length of the sources.

The outer regions of the chamber were highly irradiated compared to the centre region. The dose rate near the chamber wall can reach up to 140% of the dose rate at the centre in the same radial plane. Figure 8 displays isodose curve that is showing the dose distribution in the XZ plane. This tally described the non-uniform distribution in the radial and axial planes. Both figures demonstrate a clear trend, the dose rate is highest along the central plane of the chamber and decreases toward the top and bottom levels, while exhibiting an increase radially toward the edges of the chamber. Concerning certain regions within the chamber that inevitably have a higher dose rate, it is recommended to insert an 8 cm spacer under the chamber to raise it, and the maximum height is 21 cm from the chamber's base to achieve a dose uniformity of more than 85% relative to the maximum dose rate with a ratio of 1.1.

3.4 Transit Dose Calculation

The determination of transit dose was calculated by numerical integration utilising discrete data provided by the PHITS simulation. In this study, the calculation occurred in the middle of the chamber

by dividing the total chamber's height of 28 cm into 28 meshes, which produced Δz equal to 1 cm. T-deposit tally was set to calculate the dose rate in each mesh. The exact spatial coordinates from the experimental setup were replicated in the simulation to ensure consistency.

In this study, it was assumed that the transit dose was measured when the sample or dosimeter was positioned in the centre of the bottom of the chamber. The transit dose has a variation value that depends on the sample's location inside the chamber (Farah et al., 2025). The lower position will receive more exposure time because it enters the irradiation area earlier and leaves the irradiation area last compared to the other position. Additionally, it passes the entire height of the pencil source and is exposed for the whole dose rate along the source, which does not occur if the sample is in the middle and upper positions. As a result, the lower position will acquire a larger transit dose than the samples placed in the middle and upper positions.

The mechanical translation of the transit dose acquired in this case was when the chamber turned down and up to the irradiation field. The chamber moved at a constant speed (11.4 cm/s), corresponding to a residence time of 0.088 seconds per centimetre. The dose rate at any given point was a function of position. By applying Simpson's 1/3 rule (Equation 2), it treated the transition between 28 mesh points as a parabolic curve rather than a straight line. Due to the physical involves a complete "down and up" cycle, the integral must be multiplied by a factor of two to determine the transit dose. The final calculated values, alongside a comparative analysis with the experimental measurements are presented in Table 2.

Table 2 Transit Dose Difference between Simulation and Experimental Measurement

Category	Transit Dose (Gy)	Uncertainty (%)
PHITS Simulation	1.9	0.93
Alanine Dosimeter	1.8	2.3
RDD	2.5%	

The transit dose difference between the experimental measurement and the PHITS simulation using Simpson's rule was found to be 2.5%, demonstrating an excellent level of agreement between those two datasets.

4. Conclusion

An Observo Ignis irradiator has been modelled using the PHITS Monte Carlo code. The study successfully validated the PHITS Monte Carlo code for simulating dose distribution using experimental data. It resulted a relative agreement of less than 3%, confirming the reliability of the proposed model. These relative dose differences (RDD) indicate higher precision and accuracy than those reported in the

literature. Dose rates at the centre-axial plane (z-axis) of the chamber were ~45% lower at the bottom and top levels compared to the middle level. On the radial axis, the dose rate was higher at the edge area, as it was closer to the pencil source than at the centre area. The middle level generated the highest non-uniformity ratio compared to the top and bottom levels, producing a Dose Uniformity Ratio (DUR) of 1.4. Users of the irradiator should be aware of such inhomogeneity in dose rate distribution in the sample chamber to guarantee all samples receive a uniform dose as prescribed. To achieve a DUR equal to 1.1, the sample should be located at a height of 8 to 21 cm from the chamber's base.

The Simpson integration method was shown to be an effective numerical approach for calculating transit doses in a Category I gamma irradiator. This was evidenced by the high level of agreement with experimental data using alanine dosimeters, which yielded a relative discrepancy of less than 3%. This level of precision indicates that a quadratic polynomial approximation is sufficient for modelling the radiation field during short-duration linear transitions.

Acknowledgements

We would like to thank University of Birmingham, Lancaster University, and National Research and Innovation Agency (BRIN) for support this project.

Funding

This research received no external funding.

Data availability

Not applicable.

Declarations

Conflict of interest The authors declare no conflict of interest.

5. References

A. C. Gonçalves, J., S. R. Somessari, E., L. Somessari, S., & Bueno, C. C. (2022). Transit dose measurements using alanine and diode-based dosimeters. *Brazilian Journal of Radiation Sciences*, *10*(2A), 1–9. https://doi.org/10.15392/bjrs.v10i2a.1828

Aknouch, A., El-ouardi, Y., Hamroud, L., Sebihi, R., Mouhib, M., Yjjou, M., Didi, A., & Choukri, A. (2021). A Monte Carlo study to investigate the feasibility to use the Moroccan panoramic irradiator in sterile insect technique programs. *Radiation and Environmental Biophysics*, *60*(4), 673–679. https://doi.org/10.1007/s00411-021-00934-6

Aknouch, A., Mouhib, M., Sebihi, R., Didi, A., El-ouardi, Y., Boubekraoui, A., & Choukri, A. (2020). Monte Carlo Simulation of the Dose Rate Distribution of a Moroccan Panoramic Gamma Irradiator Using the MCNPX Code. *Moscow University Physics Bulletin*, *75*(1), 35–38. https://doi.org/10.3103/S0027134920010026

Bento, J., Barros, S., Teles, P., Neves, M., Gonçalves, I., Corisco, J., & Vaz, P. (2012). Monte carlo simulation of the movement and detection efficiency of a whole-body counting system using a bomab phantom. *Radiation Protection Dosimetry*, *148*(4), 403–413. https://doi.org/10.1093/rpd/ncr201

Chapra, S. C. ., & Canale, R. P. . (2010). *Numerical methods for engineers*. McGraw-Hill Higher Education.

Dridi, W., Daoudi, M., Farah, K., & Hosni, F. (2020). Monte Carlo validation of dose mapping for the Tunisian Gamma Irradiation Facility using the MCNP6 code. *Radiation Physics and Chemistry*, *173*(October 2019), 108942. https://doi.org/10.1016/j.radphyschem.2020.108942

El-ouardi, Y., Aknouch, A., Dadouch, A., Mouhib, M., Maghnouj, A., Benmessaoud, M., & Yjjou, M. (2023). Control of transit doses by Monte Carlo simulation inside an ionization casemate housing of a 60Co gamma irradiator. *Radiation Physics and Chemistry*, *206*(December 2022), 110776. https://doi.org/10.1016/j.radphyschem.2023.110776

Farah, K., Kuntz, F., & Hosni, F. (2025). Dosimetry characterization of Cobalt-60 self-contained dry-gamma source irradiator for nuclear sterile insect technique application. *Radiation Physics and Chemistry*, 113114. https://doi.org/10.1016/j.radphyschem.2025.113114

Feldmann, F., Shupert, W. L., Haddock, E., Twardoski, B., & Feldmann, H. (2019). Gamma irradiation as an effective method for inactivation of emerging viral pathogens. *American Journal of Tropical Medicine and Hygiene*, *100*(5), 1275–1277. https://doi.org/10.4269/ajtmh.18-0937

Firmansyah, O. A., Kurniawan, B., Walo, M., Gryczka, U., Saputro, B., Prasetio, H., Satmoko, A., & Nuraeni, N. (2025). PHITS code Monte Carlo simulation of a gamma chamber 5000. *Radiation and Environmental Biophysics*, (0123456789). https://doi.org/10.1007/s00411-025-01132-4

Fitriana, R., Putri, M. A. E., Kusuma, A. T., & Yunus, M. Y. (2024). Evaluation of Irradiation Technique to Improve Dose Uniformity in Semi-Industrial Irradiator (IRKA). *AIP Conference Proceedings*, *2967*(1). https://doi.org/10.1063/5.0192853

Follett, P. A. (2004). Irradiation to control insects in fruits and vegetables for export from Hawaii. *Radiation Physics and Chemistry*, *71*(1–2), 163–166. https://doi.org/10.1016/j.radphyschem.2004.03.074

Gual, M. R., Pereira, C., & Mesquita, A. Z. (2019). Application of a new source model of a panoramic gamma irradiator on dose map formation in an irradiated product. *Applied Radiation and Isotopes*, *144*(October 2018), 87–92. https://doi.org/10.1016/j.apradiso.2018.12.002

Guzmán Calcina, C. S., De Almeida, A., Oliveira Rocha, J. R., Abrego, F. C., & Baffa, O. (2005). Ir-192 HDR transit dose and radial dose function determination using alanine/EPR dosimetry. *Physics in Medicine and Biology*, *50*(6), 1109–1117. https://doi.org/10.1088/0031-9155/50/6/005

Hefue, J. (2000). The dose distribution inside the irradiation chamber of the gamma cell 220 at KACST using MCNP4B. *Journal of Nuclear Science and Technology*, *37*, 402–405. https://doi.org/10.1080/00223131.2000.10874915

Jecong, J. F. M., Hila, F. C., Pares, F. A., Dingle, C. A. M., Guillermo, N. R. D., Baule, A. G., & Solomon, H. M. (2022). Ob-Servo Sanguis irradiator dose mapping at the Philippine Nuclear Research Institute using MCNP5 annular ring voxels. *Radiation Physics and Chemistry*, *191*(May 2021), 109835. https://doi.org/10.1016/j.radphyschem.2021.109835

Kim, J., Moreira, R. G., & Castell-Perez, M. E. (2015). Improving phytosanitary irradiation treatment of mangoes using Monte carlo simulation. *Journal of Food Engineering*, *149*, 137–143. https://doi.org/10.1016/j.jfoodeng.2014.10.005

Majer, M., Roguljić, M., Knežević, Ž., Starodumov, A., Ferenček, D., Brigljević, V., & Mihaljević, B. (2019). Dose mapping of the panoramic 60Co gamma irradiation facility at the Ruđer Bošković Institute – Geant4 simulation and measurements. *Applied Radiation and Isotopes*, *154*(February), 108824. https://doi.org/10.1016/j.apradiso.2019.108824

Mannai, K., Askri, B., Loussaief, A., & Trabelsi, A. (2007). Evaluation using Geant4 of the transit dose in the Tunisian gamma irradiator for insect sterilization. *Applied Radiation and Isotopes*, *65*(6), 701–707. https://doi.org/10.1016/j.apradiso.2007.01.011

Moradi, F., Khandaker, M. U., Mahdiraji, G. A., Ung, N. M., & Bradley, D. A. (2017). Dose mapping inside a gamma irradiator measured with doped silica fibre dosimetry and Monte Carlo simulation. *Radiation Physics and Chemistry*, *140*(September 2016), 107–111. https://doi.org/10.1016/j.radphyschem.2017.01.032

Mortuza, M. F., Lepore, L., Khedkar, K., Thangam, S., Nahar, A., Jamil, H. M., Bandi, L., & Alam, M. K. (2018). Commissioning dosimetry and in situ dose mapping of a semi-industrial Cobalt-60 gamma-irradiation facility using Fricke and Ceric-cerous dosimetry system and comparison with Monte Carlo simulation data. *Radiation Physics and Chemistry*, *144*(June 2017), 256–264. https://doi.org/10.1016/j.radphyschem.2017.08.022

Nanez, S., & Uribe, R. M. (2023). Performance of the Harwell tape-tab alanine EPR dosimeter under typical production conditions. Effect of irradiation and storage temperature on the stability of the response. *Radiation Physics and Chemistry*, *206*. https://doi.org/10.1016/j.radphyschem.2022.110710

Oliveira, C., Salgado, J., & Ferro De Carvalho, A. (2000). Dose rate determinations in the Portuguese Gamma Irradiation Facility: Monte Carlo simulations and measurements. *Radiation Physics and Chemistry*, *58*(3), 279–285. https://doi.org/10.1016/S0969-806X(99)00462-4

Saputro, B., Saputro, A. H., Nuraeni, N., Prasetio, H., Firmansyah, O. A., Nugroho, F., & Mayditia, H. (2024). Monte Carlo Simulation As Precision Predictive Tools to Find Isodose Curve of Gamma Irradiator: A Preliminary Study. *Indonesian Journal of Applied Physics*, *14*(2), 386. https://doi.org/10.13057/ijap.v14i2.93092

Sato, T., Iwamoto, Y., Hashimoto, S., Ogawa, T., Furuta, T., Abe, S. I., Kai, T., Matsuya, Y., Matsuda, N., Hirata, Y., Sekikawa, T., Yao, L., Tsai, P. E., Ratliff, H. N., Iwase, H., Sakaki, Y., Sugihara, K., Shigyo, N., Sihver, L., & Niita, K. (2024). Recent improvements of the particle and heavy ion transport code system–PHITS version 3.33. *Journal of Nuclear Science and Technology*, *61*(1), 127–135. https://doi.org/10.1080/00223131.2023.2275736

Sato, T., Iwamoto, Y., Hashimoto, S., Ogawa, T., Furuta, T., Abe, S. ichiro, Kai, T., Tsai, P. E., Matsuda, N., Iwase, H., Shigyo, N., Sihver, L., & Niita, K. (2018). Features of Particle and Heavy Ion Transport code System (PHITS) version 3.02. *Journal of Nuclear Science and Technology*, *55*(6), 684–690. https://doi.org/10.1080/00223131.2017.1419890

Watabe, H., Sato, T., Yu, K. N., Zivkovic, M., Krstic, D., Nikezic, D., Kim, K. M., Yamaya, T., Kawachi, N., Tanaka, H., Haque, A. K. F., Islam, M. R., & Beni, M. S. (2024). Development of DynamicMC for PHITS Monte Carlo package. *Radiation Protection Dosimetry*, *200*(2), 130–142. https://doi.org/10.1093/rpd/ncad278

Wojcicka, J. B., Yankelevich, R., Trichter, F., & Fontenla, D. P. (1999). Comparison of the transit dose components and source kinematics of three high dose rate afterloading systems. *Medical Dosimetry*, *24*(1), 61–65. https://doi.org/10.1016/S0958-3947(98)00051-X